Single and double shell ignition targets for the national ignition facility at 527 nm

Wilson, Douglas Carl; Spaeth, M. L.; Yin, Lin; Sauppe, Joshua Paul; Hopkins, L. B.; Loomis, Eric Nicholas; Sacks, Ryan Foster; Albright, Brian James; Strozzi, D.; Munro, D.; Widmayer, C.; Raymond, B.; Manes, K.; Kline, John L.

To be published in: Physics of Plasmas

DOI to publisher's version: 10.1063/5.0037338

Single and Double Shell Ignition Targets for the National Ignition Facility at 527 nm

D. C. Wilson[1, a)], M. L. Spaeth[2], L. Yin[1], J. P. Sauppe[1], L. B. Hopkins[2], E. N. Loomis[1], R. F. Sacks[1], B. J. Albright[1], D. Strozzi[2], D. Munro[2], C. Widmayer[2], B. Raymond[2], K. Manes[2], and J. L. Kline[1]

[1]*Los Alamos National Laboratory, P.O. Box 1663, Los Alamos, New Mexico 87544, USA*
[2]*Lawrence Livermore National Laboratory, P.O. Box 808, Livermore California 94551, USA*
[a)]dcw@lanl.gov

Abstract. Converting and using the National Ignition Facility (NIF) to deliver 527 nm light instead of its current 351 nm would allow the laser to deliver more energy and power to ignition targets. We update previous 527 nm target design work to reflect more contemporary target designs using high-density carbon capsules and low density helium gas filled hohlraums. We extend single shell capsule designs based on current experimental results to higher energy and power and also explore double shell capsules, both driven by green light. These studies were completed using detailed pulse shapes found for targets that converged with acceptable 2-D implosion symmetries, then used the Lava Lamp II code to confirm their feasibility at NIF. A 1.2X dimensional scaleup of one tuned NIF target at the limit of its current 351 nm capabilities, shot 170827 uses 3.3 MJ, at the limit of the current NIF's 527 nm capability. With the less-structured pulse of a double shell target, 3.7 MJ could be delivered by the laser. Our LPI calculations do not preclude operation at 527 nm, particularly for low fill hohlraums, and suggest that the Stimulated Raman Backscatter may be no worse than the small quantities seen in 170827; Stimulated Forward Raman Scattering may be present. If Stimulated Brillouin Scattering is too great, the much greater laser bandwidth available at 527 nm could be used decrease backscatter. These larger targets with higher energy and power may offer a better chance of achieving ignition with only modest changes to NIF laser.

I. INTRODUCTION

Although great progress has been made toward the goal of ignition at the National Ignition Facility[1] (NIF), it has not yet been achieved. Significant DT fuel heating has been achieved[2-7], but capsule yields remain about a factor of ~15 away from ignition, defined as achieving 1 MJ of DT yield, or 3.3 10^{17} neutrons. Pak *et al.*[8] gives a summary of NIF experimental ignition campaigns. Reasons for not achieving ignition on the current NIF include implosion asymmetries, growth of perturbations from capsule mounts, fill tubes, and unknown sources increasing fuel entropy. Improvements in target design, in fabrication, and a major increase in laser energy and power may be needed to deliver increased energy to the fuel hot-spot for substantial progress. The history of ICF has been to implode large capsules with more DT fuel, to achieve higher areal density. The exception is testing physics such as convergence effects at sub-scale. (Olson *et al.*[9]) More laser energy could lead to driving larger scale targets which could achieve higher fuel compressed areal densities (ρR) without greater convergence and higher yields from greater DT mass. Higher power could lead to higher radiation temperature and higher ablation pressures. Increases in DT mass and fuel ρR could be expected to increase the ignition threshold factor and move performance closer to ignition.[10] This paper explores a few ways the higher power and energy of NIF at 527 nm could be used to reach closer to ignition.

Early glass lasers for ICF progressed from delivering 1053 nm light, to 527 nm and then to 351 nm, largely due to better absorption of laser light and lower absorption by collective plasma instabilities[11]. It was optimistically believed that large lasers could deliver enough energy and margin for ignition. However, the ~ 2MJ delivered by NIF at 351 nm has not proved adequate and upgrades to NIF's power and energy are being considered. This could entail additional fluence at 351 nm or, as considered here, changes to the laser that would enable operation at 527

nm. This paper explores using the capability of NIF to deliver more energy and power in the green, at 527 nm, rather than converting to the blue at 351 nm. Targets operating in the green were explored by Suter *et al.*[12,13] in 2004, before experiments began on NIF. Heestand *et al.* (2008)[14] reported performance of a single NIF beam operated in the green. Suter *et al* [12,13] considered gold wall hohlraums with copper doped beryllium capsules[15], the original NIF target design[16]. Since 2004 target designs have evolved, with capsules that used ablators of plastic (Glow Discharge Polymer, GDP), beryllium[17,18], and most recently, high-density carbon (HDC).[19,20,21] Hohlraum walls can now be gold or uranium. The understanding of both capsule and hohlraum physics has improved and been tested by numerous experiments[8,21,22,23,24,25,26,27,28,29]. Still a yield of 3e+17 (1 MJ produced) has not been achieved. More laser energy and power may be needed.

The energy and peak power that NIF is capable of delivering depend upon the temporal shape of the requested pulse. It is this shape that couples the target and laser together for determining optimal operation. The objective of this paper is to explore NIF capabilities at 527 nm as applied to some modern target designs, using the experience gained from previous NIF experiments at 351 nm.

NIF is fundamentally a 1053 nm laser with frequency conversion in the final optics to a shorter wavelength, either 527 nm or 351 nm. Conversion to 527 nm will allow higher laser power and higher total energy than at 351 nm. The spectral bandwidth possible at 527 nm is also much wider. The advantages at 527 nm can be exploited to deliver more energy and power to the capsule and DT fuel, potentially leading to higher neutron yields. We will explore the capabilities of NIF at 527 nm, using specific scaled target designs based on recent NIF experiments to identify laser powers and energies that would be attractive and feasible to field.

II. NIF CAPABILITIES AT 527 NM

Specific target designs need to be considered for understanding the capability of NIF at 527 nm. Energy extraction at 1053 nm and net frequency conversion both depend upon the shape of the laser pulse. Frequency conversion optics are optimized for a particular peak laser power and pulse length when most of the laser energy is delivered. A frequency converter optimized for high power will convert less efficiently at lower laser power. Single shell ignition targets require low power for an extended time at the beginning of the pulse. This feature creates a first shock in the DT fuel and sets its specific entropy profile; this is then followed by increasing the power level to drive stronger shocks that compress the capsule. Baker *et al.*[30], gives a good discussion of how the specific entropy of the fuel, the "adiabat" is defined, used, and modified in ICF targets.

Suter *et al.*[12,13] (2004) plotted the potential power and energy landscape of NIF at 1053 nm as shown by the red line in Figure 1. This curve was plotted using analytic estimates for limits to the laser within different operating regimes. It was this curve, with an assumed conversion efficiency to 527 nm of 85% (the green curve of Figure1) that captured our interest in using green for ICF experiments. We also estimated a conversion efficiency of 57% from 1053 nm to 351 nm given by the blue curve in Figure 1 (although this conversion efficiency is more sensitive to the details of the pulse shape than for conversion to 527 nm). Since 2004 laser modeling tools have improved substantially. Now when a desired 351 nm pulse is specified, the power needed at 1053 nm can be derived in an iterative process. The Laser Performance and Operations Model (LPOM)[1], with a physical optics code at its core, was developed to quantify 351 nm output from 1053 nm input as constrained by energy extraction at 1053 nm, various limits for optical damage[31], and experience with earlier NIF shots. The Optics Recycle Loop was devised to provide a supply of optics for NIF regardless of damage incurred during operation at 351 nm. Damage concerns for operation in the green are considerably lower than for operation at 351 nm, but they are by no means of no concern. Available (but unpublished) data[32] for damage initiation indicates that the fluence at 2ω is about 1.4 times higher than the fluence at 3ω for equivalent damage initiation. Data on the differences for damage growth for different wavelengths are given in Fig 7.4-4 Manes et al.[31]. Reduction of damage at 2ω compared to 3ω does not change the repetition rate of the laser because optics exchanges are not done instantly after a damage event has been observed. The size of the sites (in the range from 30 μm and larger) are monitored using the FODI system on NIF, and when their size gets large enough, as the result of damage growth, the optics exchange is done during a regular maintenance cycle. Maintenance cycles include a lot of different types of work, not just optics exchanges. An off-line version of LPOM, the Lava Lamp II code, was used to model NIF output at 527 nm for this study. When using LPOM for the green, the doubler and tripler used for analysis at 351 nm are replaced by an 18 mm thick doubler.

The 351 nm NIF shot 170827 (fielded August 27, 2017)[4], the solid blue square in Figure 1, lies close to the inferred 351nm (blue) curve and used a pulse at the limits of NIF's capabilities as reported by LPOM. This shot for the first

time produced a fusion yield twice the peak kinetic energy of the imploding shell. The high density carbon capsule was the culmination of an experimental laser tuning sequence with low laser backscatter. Higher yields and targets with substantial alpha heating have been reported.[8] The solid green markers in Figure 1 show our modeling of specific targets near the limit of the NIF capabilities, as reported by Lava Lamp II, in agreement with the green curve representing 85% conversion from 1053 nm to 527 nm.

The choice of operating points in the wide power and energy space below the solid curves relies on coupled expectations for laser and target performance. Suter et al.[12,13] populated this space with specific target designs using beryllium capsules, and gold hohlraums filled with 1.0 mg/cm^3 helium gas. More recent experience in NIF ignition experiments has led to the current typical practices of using high density carbon (HDC) shells to replace beryllium or glow discharge polymer (GDP) plastic. This has reduced the laser pulse length, improved radiation symmetry, and reduced the risk of stimulated scattering[20]. Concerns about cross beam energy transfer and stimulated backscatter led to lower hohlraum gas fill densities (now 0.03 and 0.3 vs Suter *et al.*'s 1.0 mg/cc)[21]. Capsules scaled to use more laser energy require longer laser pulses; those driven at higher hohlraum temperatures require higher laser power.

Our approach to designing single shell 527 nm targets has been to scale up targets based on NIF shot 170827 that produced 1.9e+16 neutrons, giving the fuel the same profile of specific entropy by preserving shock velocities in the DT. We also designed a capsule with a thicker ablator in the same hohlraum as 170827, but with all the power NIF could deliver at 527 nm (810TW). This led to a moderately faster implosion (438 vs 407 km/s). We did not explore increasing the fuel entropy to keep ρR constant as might be done in a Big-Foot target (e.g. Thomas et al.[28]). We have also explored double shell ignition targets which have only begun to be tested on NIF. The 527 nm double shell target is scaled from a 351nm design[33]. The qualitatively different pulse shape for a double shell capsule allows slightly more laser energy to be extracted than for a target with a single shell capsule. The capsules and hohlraums we explored are summarized in Tables I, II, and III.

FIGURE 1. Scaled NIF capabilities at 1053 nm (red), 527 nm (green) and 351 nm (blue) with specific capsule designs.

III. SCALED TARGETS AT 527NM

Table I. Characteristics of 527 nm Single Shell Targets

Capsule	170827	1.2X170827	810 TW design
Capsule Outer Radius (μm)	980	1176	999
HDC Thickness (μm)	70	84	90
DT Thickness (μm)	56	67.2	56
Solid and Gas DT density (g/cm^3)	0.25, 0.00043	0.25, 0.00043	0.25, 0.00043
Calculated Asymmetry P2/P0, P4/P0	-4 %, 11%	14%, 8%	19%, -29%
Unablated Mass (mg) Fraction (%)	201mg or 7.5%	348mg or 7.4%	211mg or 5.9%
Fuel ρR(g/cm^2) (no burn)	0.84	1.03	1.04
Peak velocity (km/s)	401	407	438
Fuel Tion (keV) (no burn)	4.0	4.0	4.7
Total Laser Energy (MJ)	1.8	3.3	1.9

To create candidates for larger, higher energy, or higher power targets at 527 nm that might have a better chance for ignition, we needed to have detailed calculations showing higher yields and better performance than at 351 nm. Our calculations of scaled targets used the two-dimensional version of the HYDRA radiation transport code[34] using

the "high-flux model"[35]. which has been extensively applied to NIF and Omega laser targets[36] We have performed hydrodynamic scaling of the entire target: the pulse length, and the capsule. Capsule and hohlraum dimensions and pulse length are scaled by a factor of X while keeping the materials the same; the laser power is scaled by X^2; and the laser energy is scaled by X^3. Since radiation transport and alpha particle transport do not scale hydrodynamically, a scaled target is only approximately tuned. We have changed to ablator thicknesses and laser pulse shapes slightly in scaled capsules to maintain the same shock pressures in the DT fuel, giving the fuels the original specific entropy profiles. With our scaling, hohlraum physics allows the time dependent radiation drive temperatures to scale closely with time. Thus, shock pressures are the same and arrival times at interfaces are scaled. In our scaled targets we have used the same laser phase plates as currently used in NIF. Since a scaled hohlraum is larger, phase plates that could produce with larger spots at the laser entrance aperture could be fabricated if lower laser intensities were desired. Laser frequencies could be adjusted to avoid cross beam transfer by operating the fundamental laser on different lines[1] or in the extreme the inner cones at 351 nm and the outer at 527 nm. With X^3 times the DT mass and X times the compressed DT areal density, the neutron yield is expected to scale by $X^{>3}$. Hurricane *et al*.[36] describe a yield scaling of velocity$^{7.67}$ times size$^{4.67}$ for fuels with the same specific entropy profiles. For an only hydrodynamically scaled target where velocity is unchanged, yield would scale as $X^{>3}$. For the 1.2XN170827 and the 810 TW design these are factors of 2.81 and 1.97. A larger capsule must also be symmetric to ignite, and may have advantages in symmetry and reduced instability growth. But these need to be calculated with alpha heating included. Our calculations of scaled 527 nm targets begin with a calculation of the high yield 351 nm targets, which are then are scaled up, while making small changes in pulse shape (tenths of a ns). The pointing of beams in the inner and outer laser cones was scaled and adjusted slightly to improve symmetry. The pulse shape and energetics for each scaled design were evaluated with Lava Lamp II to see whether they were appropriate for fielding at 527 nm on NIF.

We believe that scaling to larger size and higher fuel areal density will lead to improved target yields – the Hurricane et al[37] scaling suggests a factor of 2 or 3 increase. Areal densities both calculate and scale to increase by about 25%. But anomalous increases in fuel entropy seem to be limiting experimental areal densities[28]. This capsule physics problem could also apply at 527 nm. Thomas *et al*.[28] suggest that a scale increase of 30% or a 20% increase in fuel energy per unit mass may be needed to approach ignition. The 810TW design has a 19% increase in energy per unit mass, and the 1.2X170827 is scaled by 20%. Patel *et al*.[10] describe an experimental deficit in hot spot areal density and temperature of about 25%. Increases in total fuel rhor of 25% and corresponding increase in total areal density of the scaled designs would place these 527 nm designs much closer to ignition. However, 3D asymmetries could spoil ignition as they do now at 351 nm. Our scaled 527 nm single shell designs would represent a substantial step towards ignition, but probably not a definitive one.

IIIa. Hohlraums at 527 nm

Table II. Hohlraum Characteristics Driving Single Shell Capsules

Target	170827 (351 nm)	1.2 Times 170827 (527nm)	810 TW (527nm)
Hohlraum Diameter (μm)	620	744	620
Hohlraum Length (μm)	1120	1344	1120
Laser Entrance Hole Radius (μm)	3640	4368	3640
He Fill Gas Density (mg/cm^3)	0.3	0.3	0.3
Peak Laser Power (TW)	450	700	810
Pulse Length (ns)	7.8	9.2	6.8

(a) (b)

Figure 2. Laser pulse for 170827 (a) and resulting hohlraum radiation temperature (b) for 351nm (blue) and 527nm (green) calculations. Shown for the laser pulse are the full NIF equivalent of inner cones(blue), outer cones(red), and total (black) power.

As seen in Figure 2, the calculated radiation temperature response of hohlraums to 527 nm light is, to a good approximation, the same as that at 351 nm. Figure 2(a) shows the laser power input at 351 nm for NIF shot 170827

and for a 527 nm equivalent, and (b) the radiation temperatures in the hohlraum each produced. The four cones of NIF laser beams entering each side of the hohlraum are assigned two different laser pulses; one for the inner (23° and 30°) cones and a separate one for the outer cones (44.5° and 50°). Different powers help control the time dependent radiation symmetry on the capsule. Figure 2 shows the full NIF equivalent (192 times the single beam power) of the inner cones (blue) and outer cones (red) beams needed to produce implosion symmetry. While the radiation temperatures are not identical due to the shallower penetration of green beams, to a good approximation the radiation temperature driving the capsule is the same with 527 nm as 351 nm. This is due to almost all of the energy entering the hohlraum being absorbed, and that radiation temperature in identical hohlraums, can to a good approximation, be modeled with only the absorbed energy and pulse length[38]. To time the shocks for arrival at the identical capsule interfaces at the same scaled time, the second and third laser sub-pulses at 527 nm had to be advanced by 100 and 250 ps respectively, relatively minor changes.

To successfully model ablation pressure in the capsule, time dependent attenuation factors (laser drive multipliers) are often used[39]. In our modeling of 170827 to achieve the correct implosion time we would need a multiplier of 0.93 without backscatter subtraction (or 0.95 with) on the laser power in the final pulse. In our 527 nm simulations we have used none, not knowing what to use or when to subtract postulated backscatter. Hall *et al*.[21] show that at hohlraum gas fill densities below 0.85 mg/cm^3 there is little SRS and at 0.03 mg/cm^3 drive multipliers closer to 1.0 are needed. At 351 nm experimental observations of shock velocities, implosion velocities and implosion times can validate these multipliers. We have no such data at 527 nm, but given the similarity of calculated hohlraum temperatures, we have assumed no difference. This means that our capsule drive energies may be 5-10% to optimistic.

Implosion symmetry depends upon where the hohlraum is illuminated. The higher critical density for 351 nm than for 527 nm means that the 351 nm beams penetrate deeper into the hohlraum, causing more drive at the wall near the capsule equator. Figure 3 shows implosion symmetries of calculated capsule densities at peak yield rate for 170827 hohlraum driven at 527 (top) and 351 nm (bottom) lasers. While these cannot be directly observed as can the time integrated neutron and X-ray images or the line of sight and spectrally integrated X-ray images, they clearly show residual asymmetry remains in modes P4, P6, P8, and higher. These implosion asymmetries result from uneven laser irradiation and motion of the hohlraum wall.

Holraum fill gas density also affects where laser energy is deposited; gas pressure retards the inward motion of the hohlraum wall. Suter *et al* [12,13] used a 1.0 mg/cc fill density in all his calculations while we have used 0.3 mg/cc (as in 170827). Fills between 0.03 and 1.6 mg/cc have now been tested at NIF.

Cross beam energy transport[40] has been ignored here and could be neglected if the various laser beam cones are set to sufficiently different wavelengths. Cross beam energy transfer from the outer cone to inner cone was not needed to provide symmetry at 527 nm. If experiments at 527 nm should show a symmetry problem, cone powers could be changed, crossed beam transport invoked by adjusting laser beam frequencies, or hohlraum gas fill densities changed. Adjustments in laser spot profile, hohlruam gas fill, and cross beam energy transfer could provide additional margin to adjust and optimize implosion symmetry, but were not necessary here. It might also be possible to employ radiation shine shields as proposed by Kritcher, Robey, Young and Olson[41] to improve symmetry. In real implosions 3D asymmetries are also present and would further complicate symmetry and degrade performance. Achieving symmetry in implosions at 527 nm will require experimental tuning of gas fill, laser pointing, and cross beam transport as in now done at 351 nm.

FIGURE 3. Calculated density contours near peak compression of the 170827 capsule driven by 527 nm (top) and 351 nm (bottom) light with a hohlraum fill density of 0.3 mg/cc, no drive multipliers and no backscatter.

IIIb. Targets with Single Shell HDC Capsules

The advantage of using NIF at 527 nm instead of 351 nm is greater available energy and higher power. The greater energy could be used to field larger capsules; the higher power to field thicker, and perhaps more stable, capsules. Capsule and hohlraum imperfections, such as perturbations caused by the fill tube, and the capsule supporting structure (tent) are thought to be major impediments to ignition in both calculations[42] and experiments[42,43]. Weber *et al*.[44], found that a change from a 10 to a 5 mm diameter fill tube made a large change in the ignition parameter, but a small change in yield. Other mechanisms were degrading performance. The 20% increase in size of the scaled targets would probably make only a small difference to the growth of fill tube and perhaps other fabrication perturbations.

The recent use of HDC shells and low backscatter in NIF experiments led us to consider only HDC shells for single shell capsules, rather than doped plastic or beryllium shells that were also tested at NIF. The higher density of HDC leads to thinner shells than for different ablators with the same mass. Shocks transit the thin shells faster, leading to shorter laser pulses which in turn cause less wall motion, better symmetry, and less laser backscatter. We believe our conclusions on scaling would apply to other scaled designs, including big foot, and beryllium capsules and possibly low foot designs, but each proposed design would have to be evaluated by LAVA LAMP II for feasibility.

The 1.2 times scaled 170827 capsule and hohlraum give a close approximation to a symmetry tuned target. Lava Lamp II runs show that the 1.2 scaled pulse shape, shown in Figure 4b, is at the limit of the NIF 527 nm capability (for the assumptions made here) with a peak power of 700 TW and 3.3 MJ energy. HYDRA calculations show it ignites and produces 4.1e+18 neutrons, or 11.5 MJ. When we compare 1.2X170827 in green to a version of 170827 in blue with imposed implosion symmetry, with the shocks timed optimally, and with no drive multipliers, the neutron yield from twice the DT mass rises from 6.4 to 12 e+17, as expected. The peak fuel averaged implosion velocity decreased from 428 to 407 km/s, but the fraction of the ablator unpenetrated by the hohlraum radiation, often termed the "remaining mass fraction", rose from 4.6% to 7.4%. Radiation penetration of the ablator was less in the 527 nm target. This should lead to less ablator/fuel mixing in the larger scaled capsule. These calculations need to be taken with a caveat. With no drive multiplier our calculation of blue 170827 shows a peak radiation temperature of 314 eV, while with a 0.95 drive multiplier and as measured, the peak was only 294 eV. The increase in performance going from current 351 nm NIF to 527 nm with higher power and energy will depend on possible degradations in hohlraum temperature (e.g. drive multipliers) and on obtaining adequate symmetry. The calculations can guide us, but 527 nm experiments on hohlraum drive will be necessary.

For an alternative target that exploits the higher power available at 527 nm, we began with the hohlraum and capsule from the 170827. The peak laser power was increased to 810 TW, allowing the capsule ablator to be thickened by 20 μm. The radiation temperature reached 330 eV, above the 314 eV of the 450 TW target. The HDC mass remaining after ablation was 5.9% of the original or 211 μg in 810TW target. Only 4.6% or 125 μg remained for the 450 TW blue target, but the green target allowed 7.5% to remain. The peak fuel averaged velocity rose to 438 km/s for the 810 TW target, even though about the same ablator remained due to greater ablation pressure at the higher hohlraum temperature. This qualitative difference could lead to better confinement, breaking the velocity cliff suggested by Hurricane *et al*.[37] The relatively smaller penetration of the radiation into the ablator and higher remaining mass could lead to greater resistance to hydrodynamic instabilities[45]. The implosion velocity and unablated mass could be tuned by adjusting the HDC thickness and pulse shape. This design illustrates possible advantages with higher power alone at 527 nm.

FIGURE 4. Laser pulses (top) and capsules (bottom) for the 1.2X170827(a), 810TW HDC(b), and the Double Shell(c) target designs at 527 nm. Black is the Full NIF Equivalent Average Laser Power; Red, power in the outer beams; and Blue, power in the inner beams.

IIIc. Targets with Double Shell Capsules

Multiple shell designs have been envisioned for ignition capsules since the beginning of the ICF program. More recently they have been designed for indirect[46,47,48] and direct drive[49]on NIF. A complete double shell target with hohlraum, including the blue point shown in figure 4, as designed by E. Loomis, offers different capsule physics and different laser pulse shapes than single shell targets. In a double shell capsule like that shown in Figure 4c, the outer aluminum shell both absorbs the radiation drive and collides with the inner Be/W shell, accelerating it to modest velocities of 200-250 km/s and densities of 1000's of g/cm^3, compressing the high density DT to volume, rather than hot spot, ignition. The small size of the inner capsule leads to lower radial convergence of the fuel, but the convergence of the outer shell and its collision with the inner shell lead to strong asymmetry and instability growth. Montgomery *et al*.[33] gives detailed comparison of double and single shell capsule physics.

The high density of the inner shell and its low convergence allow the elimination of the long, low intensity foot of single shell capsules. The change to a nearly flat laser pulse, allows more energy to be extracted from NIF at 1053 nm followed by more efficient conversion to 527 nm. It also leads to little laser plasma backscatter as measured at 351 nm[50]. Although the 351 nm double shell target uses the maximum NIF power, we have not explored the yet higher power available in 527 nm designs. These could be the subject of a future paper. The physics of the double shell capsules and their hohlraums are being tested now[50] on NIF, but a DT filled double shell target has not yet been fielded. We have scaled up the 351 nm fall line optimized target described by Montgomery *et al.*[33] by a dimensional

factor of 1.27. and used the laser cone pulse shapes in Figure 4c to achieve a target at 527 nm. Lava Lamp II calculations show that its 3.66 MJ laser energy is near the limit of the capabilities of NIF at 527 nm. Both the 351 and 527 nm double shell targets are shown in Figure 1. The 527 nm target can extract more total energy than the 1.2X17027 single shell target. This double shell target calculates to give an output of 2.6 MJ, or 9.3e+17 neutrons. The peak radiation drive temperature is 322 eV, similar to the 318 eV of the 1.2X170827 target, and the 330 eV of the 810 TW HDC single shell target.

Table III. Characteristics of Double Shell Targets

Target	1.8 MJ 351 nm	3.66 MJ 527nm
Capsule Outer Radius (μm)	1095	1386
Aluminum Thickness (μm)	154	195
DT Thickness (μm)	214	271
DT Density (g/cm^3)	0.20	0.20
Hohlraum Diameter (μm)	575	728
Hohlraum Length (μm)	1040	1316
Laser Entrance Hole Diam(μm)	1344	1700
He Fill Gas Density (mg/cm^3)	0.3	0.3
Mean Peak Laser Power (TW)	500	800
Pulse Length (ns)	4.9	6.2

IV. ASSESSMENT OF LASER PLASMA INSTABILTIY RISKS

The historical progression of ICF lasers has been in the direction of shorter wavelength—from 10,000 nm, to 1053 nm, and then to 351 nm—in order to reduce laser plasma instability growth. In those times the energy NIF could supply at 351 nm was thought to adequate to achieve ignition. Increasing NIF's delivered energy and regressing to 527 nm might lead to greater laser plasma instability growth and backscatter. In particular, problematic levels of stimulated Brillouin scattering (SBS) and stimulated Raman scattering (SRS) might arise, although the laser damage from 527 nm SBS would be less than for 351 nm SBS. The change from targets with plastic and beryllium ablators to HDC has shortened the pulse, and the reduction of hohlraum helium gas fill density from 1.6 to 0.3 mg/cm^3 has substantially reduced both SBS and SRS backscatter at 351 nm. Hohlraums at 0.3 mg/cc show little SRS and SBS[21]. For example, the measured backscatter was low on 170827: the total backscattered energy fraction was 2.2%; none on the 23° cone and 0.95% SRS on the 30° inner cones; 3.5% SBS on the 50° cones with 0.95% SRS and 0.78% SBS on the 44° outer cones. Forward SRS has been measured[51], but not for this target. Hot electron pre-heat generated by SRS was insignificant. This suggests the possibility that there may be LPI margin at 351 nm, and that our 527 nm designs might have acceptably low backscatter levels. Because of the low measured backscatter at 351 nm, we have, optimistically, neglected it in our 527 nm simulations, neither subtracting it from laser beam power, nor including hot electron generated pre-heat. Energetically, we might expect backscatter to be insignificant; any loses could be compensated for by slightly increasing laser power.

To evaluate the risk of LPI backscatter, we have performed backward and forward stimulated Raman scattering (BSRS and FSRS) using the particle-in-cell code VPIC[52,53,54]. We begin our simulations of LPI with a discussion of simulations using blue and green light in a uniform plasma, then blue light simulations of NIF shot 170827 in its hohlraum, comparing with observed backscatter, and finally green light simulations of 1.2X170287.

For the VPIC simulations in this work, the cell size is approximately the Debye length and 512 particles per cell are used for each species. We expect these results to be converged based on the requirements of the PIC method and our prior studies modeling LPI under NIF hohlraum conditions. Moreover, both the level of Langmuir wave thermal fluctuations and the level of collective Thomson scatter from Langmuir waves in these VPIC simulations are close to those in the physical system (Yin et al.[55]). The simulation box size is sufficiently long (1mm - 2mm) that BSRS initiated in one region would be amplified in other regions as the scattered light convects in the simulation domain. Although the scattered light can be re-amplified outside the simulation domain in the LEH (Kirkwood *et al.*[56,57]), the increased damping of the backscattered light in the LEH region plasma would likely limit the growth, making these simulations appropriate to evaluate the dominant LPI processes.

2D VPIC simulations in uniform plasma were performed to compare BSRS and FSRS with green and blue light. The laser beam was modeled with a random phase plate (RPP) beam with an optical F/# of 8 and average intensity $3\text{x}10^{14}$ W/cm^2. The simulation box is 751 μm by 120 μm in (*x, z*) with 120 μm laser beam width in green (Run7-1), and 500μm by 80μm in (*x, z*) with 80 μm laser beam width in blue (Run7-2). For both green and blue lasers, the plasma has density 0.12 n_{cr} and electron temperature T_e = 2.6 keV, and the RPP beams have frequency ω_0/ω_{pe}=2.88 (ω_{pe} is the plasma frequency). The simulations parameters are chosen such that the simulation box size, the laser beam width, and the speckle length and width are the same in units of Debye length and laser wavelength. From linear theory, BSRS is at $k\lambda_D$=0.3. Another simulation has green light with the same box size but with reduced beam width of 60 μm (Run7-3) to examine sensitivity of Raman scattering to beam size.

Figure 5 shows the time-averaged BSRS reflectivity and the hot electron energy spectrum for the three simulations, with solid curves for Run7-1 (green light), dashed curves for Run7-2 (blue light), and dash-dot curves for Run7-3. With blue light, no significant FSRS occurs and the highest hot electron energy is ~100 keV; with green light, oblique FSRS is unstable and its hot electron energy is higher than that from BSRS and it increases with laser beam width (reaching up to 250 keV) as a result of speckle coupling (SRS initiated in a high intensity speckle can seed SRS in nearby, lower-intensity speckles via scattered light waves, hot electrons, and plasma waves[55,58]). Based on 1D theory[59], the FSRS growth rate is

$$\gamma \cong \frac{\omega_{pe}^2}{2\sqrt{2}\omega_0}\frac{v_{os}}{c} = \frac{1}{2\sqrt{2}}\frac{eE_0}{m_e c}\frac{n_e}{n_{cr}},$$

where $v_{os} = eE_0/m_e\omega_0$ is the electron quiver velocity in laser amplitude E_0. The two simulations Run7-1 and Run7-2 have the same laser intensity and plasma density n_e/n_{cr} and thus should have the same FSRS growth rate γ. The higher level of FSRS with green light cannot be explained by 1D theory where the scattered light is in the direction of the laser, whereas the FSRS seen in the 2D hohlraum simulations are oblique. As a consequence of the FSRS, the growth of BSRS is suppressed as indicated in Figure 5 (a) in which the solid curve drops as FSRS grows. As the laser beam width and FSRS are reduced, the reflectivity in Run7-3 further increases.

FIGURE 5. 2D VPIC simulations in uniform plasmas comparing BSRS and FSRS with green and blue light. Run7-1 (green light), solid curves; Run7-2 (blue light), dash curves; and Run7-3, dash-dot curves (green light smaller laser beam width) (a) Time-averaged BSRS reflectivity. (b) Hot electron energy spectrum (dot curve is the initial Maxwellian spectrum).

To test the ability of VPIC simulations to reproduce NIF experiments, simulations using the plasma conditions from the HYDRA simulation of 170827 with blue light were performed to compare with the experimental measurements of Raman scattering. Large-scale VPIC simulations of hohlraum plasma with NIC design and with designs using diamond capsules have been performed to assess the LPI risks using plasma conditions from the HYDRA code using an initial hohlraum gas fill of 0.30 mg/cm^3; in these studies, modeled SRS reflectivity and spectra are consistent with those measured (Yin et al.[58,60]) For these VPIC simulations, the laser beam was modeled with a RPP beam with an optical F/# of 8 and average intensity 3.0x10^{14} W/cm^2 and the same laser pointing as the HYDRA simulations. We also introduced electron collisionality. In the VPIC simulation, the plasma density is initialized with a spatially varying function obtained from fitting the HYDRA simulation data, whereas the plasma temperature is spatially uniform based on the spatially averaged value from the HYDRA data over the region modeled in VPIC. Temperature variations from HYDRA output across the volume simulated in VPIC are minimal, justifying this approximation. The plasma for the simulation box along the 30° beam path has average electron temperature T_e=3.1keV, maximum density n_e/n_{cr}=0.22 (n_{cr} is the respective critical density), and minimum $k\lambda_D$=0.18 for BSRS. On the 50° beam path, the average electron temperature is T_e=5keV, the maximum density n_e/n_{cr}=0.2, and the minimum $k\lambda_D$=0.26 for BSRS. The box size is 1000 μm by 600 μm in (x, z) and the laser beam width is 600 μm for the four simulations along the 30° and 50° beam paths with and without collisions. Figure 6(a) shows the hohlraum density, indicating regions of the simulation domains. Reflectivity along the 50° beam path is ~1.4% for both simulations with and without collisions, in agreement with the low reflectivity in the experimental data. However, the reflectivity from the simulation along the 30° beam path is >25% both with and without collisions, significantly higher than the experimental data. The estimated inverse bremsstrahlung damping of the laser beam is small, as confirmed by the VPIC simulations. The collisional effects on the reflectivity are small, however FSRS hot electron is reduced by collisions as indicated by results in frame (d). This raises concerns about the accuracy of the plasma conditions from HYDRA simulation in high density-gradient region along the inner beam path of the 30° beam.

FIGURE 6. 2D VPIC simulations of BSRS using plasma conditions from the 170827 blue light HYDRA simulation. Shown in (a) are contours of the hohlraum plasma density at 7ns at the peak of the laser pulse with black lines indicating the 23º, 30º, 44º, and 50º beam paths; VPIC simulation domains are indicated by the shaded areas along the 30º and 50º beam paths (the blue dots are the center of the simulation boxes). (b) Time-averaged BSRS reflectivity along the 30º (b) and 50º beam (c). (d) Hot electron energy spectrum from simulation along the 50º beam. The solid curves in (b), (c), and (d) are from collisionless simulations, while the dash curves are from collisional simulations; the dot curve in (d) is the initial Maxwellian spectrum.

In our assessments of SRS in the green light 1.2X170827, target plasma density and temperature profiles obtained from HYDRA green light simulations are employed. Figure 7(a) shows the contours of BSRS $k\lambda_D$ values of the hohlraum plasma at 6 ns at the peak of the laser pulse with a shaded region along the inner beam paths indicating maximum domain size of the VPIC simulations with parameters summarized in Table 1. The simulations are performed with and without collisions and laser bandwidth, the latter intended to explore mitigation options for SRS.

TABLE IV. 2D VPIC simulation parameters using hohlraum plasma conditions at 6 ns from 1.2X170827 green light design shown in Figure 7 (a). Run5-8 and Run5-9 use the same bandwidth but with two different random seeds for generating the laser beam.

Simulation name	Box size in x (μm)	Box size in z (μm)	Beam width (μm)	Collisions	Laser bandwidth (THz)	Ave. T_e (keV)	Max n_e/n_{cr}	Min $k\lambda_D$ (BSRS)

Run5-1	1000	600	300	No	0	1.8	0.068	0.36
Run5-2	1000	600	600	No	0	1.8	0.068	0.36
Run5-3	1000	300	280	No	0	1.8	0.048	0.45
Run5-4	1000	300	150	No	0	1.8	0.048	0.45
Run5-5	1000	300	150	No	0.156	1.8	0.048	0.45
Run5-6	1000	300	150	No	15.6	1.8	0.048	0.45
Run5-7	1800	1000	1000	No	0	1.96	0.078	0.34
Run5-8	1800	1000	1000	No	3.0	1.96	0.078	0.34
Run5-9	1800	1000	1000	No	3.0	1.96	0.078	0.34
Run5-10	1800	1000	1000	Yes	0	1.96	0.078	0.34

Of the ten simulations, Run5-1 and Run5-2 are medium-size simulations with the same box sizes of 1000μm by 600 μm in (x, z) but with a laser beam width of 300 μm and 600 μm, respectively. They show similar, low levels of reflectivity (~2%) in Figure 7(b), comparable to the measured blue 170827 reflectivity levels. However, with green light, oblique FSRS[61] is unstable in these two simulations: frame (c) shows the hot electron energy spectrum with maximum energy ~400 keV and frame (g) shows the electron velocity space distribution $f(v_x, v_z)$, indicating electron trapping in FSRS daughter electron plasma wave (EPW).

To examine the sensitivity of FSRS dependence on laser beam width, Run5-3 and Run5-4 are performed in which the simulation size is reduced to 1000 μm by 300 μm in (x, z) with 280μm and 150μm beam widths, respectively. The BSRS levels in these simulations are insignificant and Figure 7(d) shows that FSRS hot electron production decreases with beam width (comparing the black and red curves). Furthermore, Run5-5 and Run5-6 are performed with the same box size and beam width as Run5-4 but with laser bandwidths of 0.156 THz and 15.6THz, respectively. Results in Figure 7(d) shows the suppression of FSRS hot electrons by laser bandwidth (comparing the red, blue, and green curves). Since SRS occurs on a fast electron time scale, the required laser bandwidth for mitigation is high, higher than available from NIF (even with new modulators) even after the exchange of frequency converters from blue to green.

At larger spatial scales, simulations are performed with box size 1800 μm by 1000 μm in (x, z) and laser beam width 1000 μm, but without collisions and bandwidth (Run5-7), without collisions but with 3 THz bandwidth (Run5-8 and Run5-9 using two different random seeds in generating the laser beams), and with collisions but without bandwidth (Run5-10). Surprisingly, the BSRS reflectivity from Run5-7 is ~30%, significantly higher than in the smaller size runs discussed above. The SRS is also strongly nonlinear and insensitive to collisions [comparing solid and dotted curves in Figure 7(e)]. With 3THz laser bandwidth, the BSRS reflectivity is reduced to ~10%. Figure 7(f) shows the SRS hot electron spectrum from these runs: the 3THz laser bandwidth reduces FSRS hot electrons (comparing the solid curve without bandwidth and the dash and dash-dot curves with bandwidth); however, collisions are more effective in suppressing FSRS hot electrons because the FSRS daughter EPW has large phase velocity and interacts with the tail of the electron distribution [indicated in frame (g)]. As seen in the uniform plasma simulations with green light, oblique FSRS is present as illustrated by the example in Figure 7 (g).

Future assessment of FSRS mitigation using bandwidth should include collisions. The high reflectivity results from the largest scale simulations that have a domain indicated by the shaded box in Figure 7(a) where a high gradient region is included (whereas this is excluded in the six smaller scale simulations Run5-1 to Run5-6). In this thin region of high density gradient, the density jumps abruptly by more than 20% over tens of microns. The density scale length is $L_n \sim 1/(d \log n/dx) \sim 20\ \mu m / (0.2) \sim 100\ \mu m$. The mean free path for ion-ion collisions is ~5 microns (for electron-electron collisions, ~50 μm). This implies a Knudsen number 0.05 (0.5), well within the regime where kinetic modifications to the hydrodynamic equations become important. Therefore, the HYDRA code is likely not modeling properly the inter-penetration of the counter-streaming plasmas. While this may not affect the fusion yield appreciably (capsule dynamics integrate the x-ray radiation drive from the hohlraum, which is largely insensitive to these details), it does however lead to differences in the hohlraum plasma conditions, which can in turn affect the LPI. Consequently, LPI assessments based upon simulations over domains containing these possibly unphysical features are not likely to be predictive.

FIGURE 7. 2D VPIC simulations assessing BSRS and FSRS risks using plasma conditions from 1.2X170827 green light design. Shown in (a) are contours of BSRS $k\lambda_D$ values of the hohlraum plasma at 6ns at the peak of the laser pulse with black lines indicating the 23°, 30°, 44°, and 50° beam paths; VPIC simulations of domain sizes up to the shaded area (the blue dot is the center of the simulation boxes) are performed (see Table 1). (b) Time-averaged BSRS reflectivity (b) hot electron energy spectrum (c) from Run5-1 (solid curves) and Run5-2 (dash curves). (d) Hot electron energy spectrum from Run5-3 (black), Run5-4 (red), Run5-5 (blue), and Run5-6 (green). Time-averaged BSRS reflectivity (e) and hot electron energy spectrum (f) from Run5-7 (solid curves), Run5-8 and Run5-9 (dash and dash-dot curves), and Run5-10 (dot curves). (g) Electron velocity space distribution $f(v_x, v_z)$ showing excitation of the oblique FSRS. The dot curves in (c) and (f) are the initial Maxwellian spectra.

In summary, the VPIC simulations of BSRS in moderately large domains show low levels of reflectivity (~2% or smaller), suggesting it may not be a problem for these green target designs; on the other hand, VPIC simulations performed over the largest spatial scale indicate significantly higher reflectivity level (~30%) than in the smaller size simulations. Furthermore, VPIC simulations show that oblique FSRS may arise with the green light option (at a more significant level than with the blue light), leading to hot electron production. Increasing laser bandwidth may reduce hot electron production. Larger and more detailed simulations may be needed, emphasizing the need for 527 nm LPI experiments. We note that the LPI assessment in this work (and in other work using various LPI tools in the community) relies on plasma conditions from hohlraum hydrodynamic simulations that may not represent correctly the interpenetration of counter-streaming plasmas which may be necessary for accurately predicting LPI levels, especially at largest special scale. In the future, with focused, well-diagnosed LPI experiments available in smaller laser facilities, the degree of accuracy of the plasma conditions predicted by rad-hydro design codes can be evaluated.

The largest backscatter threat to experiments at 351 nm is SBS and, we hypothesize, this may also be the case at 527 nm. VPIC simulations on longer timescale may be performed in the future to provide assessment on SBS risk. The frequency change to 527 nm may also enable another option for control. Large laser bandwidth can also suppress instability growth, particularly SBS[62]. At the present time, NIF has a bandwidth of 45-90 GHz at 1053 nm, corresponding to 135-270 GHz in the blue. The bandwidth in the blue is constrained by a reduction in conversion efficiency as the bandwidth is increased. This same effect does not occur in the green where the bandwidth is only constrained by the linewidth, now ~0.50 THz [63], of the 1053 nm amplifiers. The available bandwidth in the green is then ~1.0 THz, Realization of this much larger bandwidth would require new modulators to be added to NIF. A large bandwidth of $\Delta\nu/\nu$=2% at 527 nm was demonstrated in a frequency doubled Nd:glass laser by Eimerl *et al.*[64]. Cross-beam energy transfer may also be mitigated by such enhanced bandwidth[65].

While simulations can give guidance, hohlraum experiments conducted at 527 nm to measure SRS and SBS would be invaluable for discovering whether high backscatter exists and characterizing it.

V. CONCLUSIONS

Several target types and their corresponding capabilities have been evaluated when driven by a NIF laser that has been converted to operate at 527 nm rather than 351 nm. Results are encouraging, with the most straight-forward path following that first established by 170827 at 351 nm. In general, operating NIF in the green should allow larger capsules to be fielded. These may make the effects of fill tube imperfections, capsule support structures, and capsule surface imperfections less significant. The fidelity of laser plasma instability modeling is such that experiments at 527 nm will be required to test performance at extrapolated sizes. Our LPI calculations do not preclude operation at 527 nm, particularly for low fill hohlraums, and the potential benefits to power and energy justify experimental tests. This will probably be done before NIF is converted from 351 to 527 nm. Our radiation hydrodynamic calculations suggest that the current NIF 1053 nm laser, converted to green, could drive hohlraums with single shell HDC capsules using 3.3 MJ or perhaps 3.7 MJ with double shell targets. The 20% larger HDC

capsules and the 810TW high power design should achieve higher yields and higher fuel areal densities. The upgrade of NIF to a 527 nm laser on target would be a substantial, but probably not a definitive, step toward ignition. If NIF's 1053 nm power and energy could be further increased, then yet larger capsules could be fielded. We agree with D. S. Clark *et al.*[42], "Given the uncertainties in any extrapolation, particularly as nonlinear as ignition, there will be no definitive answer on the requirements for ignition until it is actually demonstrated experimentally". This is also true at 527 nm.

ACKNOWLEDGMENTS

The authors would like to acknowledge the efforts of the NIF operations, laser performance, target diagnostics, and target fabrication teams. The Lava Lamp II team built the important software needed to evaluate the feasibility of our proposed laser pulses at NIF. The Los Alamos LPI work was supported by the ICF program and Advanced Simulation and Computing (ASC) program. VPIC simulations were run on ASC Trinity supercomputer under Capability Class Computing and the Large-Scale Calculations Initiative (LSCI). This work was also performed under the auspices of the U.S. Department of Energy by Los Alamos National Laboratory under Contract No. DE-AC52-06NA25396 and by Lawrence Livermore National Laboratory under Contract No. DE-AC52-07NA27344. This document (LA-UR-20-29072) was prepared as an account of work sponsored by an agency of the United States government. Neither the United States government nor Lawrence Livermore National Security, LLC, nor any of their employees makes any warranty, expressed or implied, or assumes any legal liability or responsibility for the accuracy, completeness, or usefulness of any information, apparatus, product, or process disclosed, or represents that its use would not infringe privately owned rights. Reference herein to any specific commercial product, process, or service by trade name, trademark, manufacturer, or otherwise does not necessarily constitute or imply its endorsement, recommendation, or favoring by the United States government or Lawrence Livermore National Security, LLC. The views and opinions of authors expressed herein do not necessarily state nor reflect those of the United States government nor Los Alamos National Security, nor Lawrence Livermore National Security, LLC, and shall not be used for advertising or product endorsement purposes. The data that supports the findings of this study are available within the article or from the corresponding author on reasonable request.

REFERENCES

1M. L. Spaeth, K. R. Manes, D. H. Kalantar, P. E. Miller, J. E. Heebner, E. S.Bliss, D. R. Spec, T. G. Parham, P. K. Whitman, P. J. Wegner, P. A. Baisden, J. A. Menapace, M. W. Bowers, S. J. Cohen, T. I. Suratwala, J. M. Di Nicola, M. A. Newton, J. J. Adams, J. B.Trenholme, R. G. Finucane, R. E. Bonanno, D. C. Rardin, P. A. Arnold, S. N. Dixit, G. V. Erbert, A.C. Erlandson, J. E. Fair, E. Feigenbaum, W. H. Gourdin, R. A. Hawley, J. Honig, R. K. House, K.S. Jancaitis, K. N. LaFortune, D. W. Larson, B. J. Le Galloudec, J. D. Lindl, B. J. MacGowan, C. D.Marshall, K. P. McCandless, R. W. McCracken, R. C. Montesanti, E. I. Moses, M. C. Nostrand, J.A. Pryatel, V. S. Roberts, S. B. Rodriguez, A. W. Rowe, R. A. Sacks, J. T. Salmon, M. J. Shaw, S. Sommer, C. J. Stolz, G. L. Tietbohl, C. C. Widmayer & R. Zacharias, Fusion Science and Technology **69**, 25-145 (2016).

2O. A. Hurricane, D. A. Callahan, D. T. Casey, E. L. Dewald, T. R. Dittrich, T. Doppner, S .Haan, D. E. Hinkel, L.F. Berzak Hopkins, O. Jones, A.L. Kritcher, S. Le Pape, A. Ma, A. G. MacPhee, J. L. Milovich, J. Moody, A. Pak, H.-S. Park, P. K. Patel, J. E. Ralph, H. F. Robey, J. S. Ross, J. D. Salmonson, B. K. Spears, P. T. Springer, R. Tommasini, F. Albert, L. R. Benedetti, R. Bionta, E. Bond, D. K. Bradley, J. Caggiano, P. M. Cellers, C. Cerjan, J. A.

Church, R. Dylla-Spears, D. Edgell, M. J. Edwards, D. Fittinghoff, M. A. Barrios Garcia, A. Hamza, R. Hatarik, H. Herrmann, M. Hohenberger, D. Hoover, J. L. Kline, G. Kyrala, B. Kozioziemski, G. Grim, J. E. Field, J. Frenje, N. Izumi, M. Gatu Johnson, S. F. Khan, J. Knauer, T. Kohut, O. Landen, F. Merrill, P. Michel, A. Moore, S. R. Nagel, A. Nikroo, T. Parham, R. R. Rygg, D. Sayre, M. Schneider, D. Shaughnessy, D. Strozzi, R. P. J. Town, D. Turnbull, P. Volegov, A. Wan, K. Widmann, C. Wilde, and C. Yeamans, Nat. Phys **12**, 800-806 (2016).

3N. B. Meezan, M. J. Edwards, O. A. Hurricane, P. K. Patel, D. A. Callahan, W. W. Hsing, R. P. J. Town, F. Albert, P. A. Amendt, L. F. Berzak Hopkins, D. K. Bradley, D. T. Casey, D. S. Clark, E. L. Dewald, T. R. Dittrich, L. Divol, T. Doppner, J. E. Field, S. W. Haan, G. N. Hall, B. A. Hammel, D. E. Hinkel, D. D. Ho, M. Hohenberger, N. Izumi, O. S. Joes, S. F. Khan, J. L. Kline, A. L. Kritcher, O. L. Landen, S. LePape, T. Ma, A. J. McKinnon, A. G. MacPhee, L. Masse, J. L. Masse, J. L. Milovich, A. Nikroo, A. Pak, H-S. Park, J. L. Peterson, H. F. Robey, J. S. Ross, J. D. Salmonson, V. A. Smalyuk, B. K. Spears, M. Stadermann, L. J. Suter, C. A. Thomas, R. Tommasini, D. P. Turnbull, and C. R. Weber, Plasma Phys. Control. Fusion 59, 014021 (2017).

4S. Le Pape, L. F. Berzak Hopkins, L. Divol, A. Pak, E. L. Dewald, S. Bhandarkar, L. R. Bennedetti, T. Bunn, J. Biener, J. Crippen, D. Casey, D. Edgell, D. N. Fittinghoff, M. Gatu-Johnson, C. Goyon, S. Haan, R. Hatarik, M. Havre, D. D-M. Ho, N. Izumi, J. Jaquez, S. F. Khan, G. A. Kyrala, T. Ma, A. J. Mackinnon, A. G. MacPhee, B. J. MacGowan, N. B. Meezan, J. Milovich, M. Millot, P. Michel, S. R. Nagel, A. Nikroo, P. Patel, J. Ralph, J. S. Ross, N. G. Rice, D. Strozzi, M. Stademann, P. Volegov, C. Yeamans, C. Weber, C. Wild, D. Callahan, and O. A. Hurricane, Phys. Rev. Lett. **120**, 245003 (2018).

5L. Berzak Hopkins, S. LePape, L. Divol, A. Pak, E. Dewald, D. D. Ho, N. Meezan, S. Bhandarkar, L. R. Benedetti, T. Bunn, J Biener, J Crippen, D Casey, D Clark, D Edgell, D Fittinghoff, M Gatu-Johnson, C Goyon, S Haan, R Hatarik, M Havre, D Hinkel, H Huang, N Izumi, J Jaquez, O Jones, S Khan, A Kritcher, C Kong, G Kyrala, O Landen, T Ma, A MacPhee, B MacGowan, A J Mackinnon, M Marinak, J Milovich, M Millot, P Michel, A Moore, S R Nagel, A Nikroo, P Patel, J Ralph, H Robey, J S Ross, N G Rice, S Sepke, V A Smalyuk, P Sterne, D Strozzi, M Stadermann, P Volegov, C Weber, C Wild, C Yeamans, D Callahan, O Hurricane, R P J Town and M J Edwards, Plasma Phys. Control. Fusion 61, 014023 (2018).

6J. L. Kline, S. H. Batha, L. R. Benedetti, D. Bennett, S. Bhandarkar, L. F. Berzak Hopkins, J. Biener, M. M. Biener, R. Bionta, E. Bond, D. Bradley, T. Braun, D.A. Callahan, J. Caggiano, C. Cerjan, B. Cagadas, D. Clark, C. Castro, E.L. Dewald, T. Döppner, L. Divol, R. Dylla-Spears, M. Eckart, D. Edgell, M. Farrell, J. Field, D.N. Fittinghoff, M. Gatu Johnson, G. Grim, S. Haan, B.M. Haines, A.V. Hamza, EP. Hartouni, R. Hatarik, K. Henderson, H.W. Herrmann, D. Hinkel, D. Ho, M. Hohenberger, D. Hoover, H. Huang, M.L. Hoppe, O.A. Hurricane, N. Izumi, S. Johnson, O.S. Jones , S. Khan, B.J. Kozioziemski, C. Kong, J. Kroll, G.A. Kyrala, S. LePape, T. Ma, A.J. Mackinnon, A.G. MacPhee, S. MacLaren, L. Masse, J. McNaney, N.B. Meezan, J.F. Merrill, J.L. Milovich, J. Moody, A. Nikroo, A. Pak, P. Patel, L. Peterson, E. Piceno, L. Pickworth, J.E. Ralph, N. Rice,

H.F. Robey, J.S. Ross, J.R. Rygg, M.R. Sacks, J. Salmonson,
D. Sayre, J.D. Sater, M. Schneider, M. Schoff, S. Sepke, R. Seugling,
V. Smalyuk, B. Spears, M. Stadermann, W. Stoeffl, D.J. Strozzi,
R. Tipton, C. Thomas, RPJ Town, P.L. Volegov, C.Walters, M. Wang,
C. Wilde, E. Woerner, C. Yeamans, S.A. Yi, B. Yoxall, Nuclear Fusion, 59, 112018 (2019).

7K. L. Baker, C. A. Thomas, D. T. Casey, M. Hohenberger, S. Khan, B. K. Spears, O. L. Lander, R. Nora, D. T. Woods, J. L. Milovich, R. L. Berger, D. Strozzi, C. Weber, D. Clark , O. A. Hurricane , D. A. Callahan, A. L. Kritcher, B. Bachmann , L. R. Benedetti, R. Bionta, P. M. Celliers, D. Fittinghoff, C. Goyon, R. Hatarik, N. Izumi, M. Gatu Johnson, G. Kyrala, T. Ma , K. Meaney, M. Millot , S. R. Nagel , P. K. Patel , D. Turnbull, P. L. Volegov , C. Yeamans, and C. Wilde, Phys. Rev. E, **102**, 023210 (2020).

8A. Pak, L. Divol, C. R. Weber, L. F. Berzak Hopkins, D. S. Clark, E. L. Dewald, D. N. Fittinghoff, V. Geppert-Kleinrath, M. Hohenberger, S. Le Pape, T. Ma, A. G. MacPhee, D. A. Mariscal, E. Marley, A. S. Moore, L. A. Pickworth, P. L. Volegov, C. Wilde, O. A. Hurricane, and P. K. Patel, Phys. Rev. Letters, 124, 145001, (2020)

9R E Olson, R J Leeper, S A Yi, J L Kline, A B Zylstra, R R Peterson, R Shah, T Braun, J Biener, B J Kozioziemski, J D Sater, M M Biener, A V Hamza, A Nikroo, L Berzak Hopkins, D Ho, S LePape and N B Meezan, Journal of Physics: Conference Series 717 012042 (2016)

10P. K. Patel, P. T. Springer, C. R. Weber, L. C. Jarrott, O. A. Hurricane, B. Bachmann, K. L. Baker, L. F. Berzak Hopkins, D. A. Callahan, D. T. Casey, C. J. Cerjan, D. S. Clark, E. L. Dewald, L. Divol, T. Döppner, J. E. Field, D. Fittinghoff, J. Gaffney, V. Geppert-Kleinrath, G. P. Grim, E. P. Hartouni, R. Hatarik, D. E. Hinkel, M. Hohenberger, K. Humbird, N. Izumi, O. S. Jones, S. F. Khan, A. L. Kritcher, M. Kruse, O. L. Landen, S. Le Pape, T. Ma, S. A. MacLaren, A. G. MacPhee, L. P. Masse, N. B. Meezan, J. L. Milovich, R. Nora, A. Pak, J. L. Peterson, J. Ralph, H. F. Robey, J. D. Salmonson, V. A. Smalyuk, B. K. Spears, C. A. Thomas, P. L. Volegov, A. Zylstra, and M. J. Edwards. , Phys. Plasmas 27, 050901 (2020).

11J. H. Nuckolls, Phys. Today, 35, 24-31 (1982).

12L. J. Suter, S. Glenzer, S. Haan, B. Hammel, K. Manes, N. Meezan, J. Moody, M. Spaeth, L. Divol, K. Oades, and M. Stevenson, Phys. Plasmas **11**, 2738-2745 (2004).

13L. J. Suter, S. Glenzer, S. Haan, B. Hammel, K. Manes, N. Meezan, J. Moody, M. Spaeth, K. Oades, and M. Stevenson, Nucl. Fusion **44**, S140-S148 (2004)

14G. M. Heestand, C. A. Haynam, P. J. Wegner, M. W. Bowers, S. N. Dixit, G. V. Erbert, M. A. Henesian, M. R. Hermann, K. S. Jancaitis, K. Knittel, T. Kohut, J. D. Lindl, K. R. Manes, C. D. Marshall, N. C. Mehta, J. Menapace, E. Moses, J. R. Murray, M. C. Nostrand, C. D. Orth, R. Patterson, R. A. Sacks, R. Saunders, M. J. Shaw, M. Spaeth, S. B. Sutton, W. H. Williams,

C. C. Widmayer, R. K. White, P. K. Whitman, S. T. Yang, and B. M. Van Wonterghem, Appl. Optics **47**, 3494-3499 (2008).

15D. C. Wilson, P. A. Bradley, N. M. Hoffman, F. J. Swenson, D. P. Smitherman, R. E. Chrien, R. W. Margevicius, D. J. Thoma, L. R. Foreman, J. K. Hoffer, S. R. Goldman, S. E. Caldwell, T.R. Dittrich, S. W. Haan, M. M. Marinak, S. M. Polaine, and J. J. Sanchez, Phys. Plasmas 5, 1953 (1998).

16S. W. Haan, J. D. Lindl, D. A. Callahan, D. S. Clark, J. D. Salmonson, B. A. Hammel, L. J. Atherton, R. C. Cook, M. J. Edwards, S. Glenzer, A. V. Hamza, S. P. Hatchett, M. C. Herrmann, D. E. Hinkel, D. D. Ho, H. Huang, O. S. Jones, J. Kline, G. Kyrala, O. L. Landen, B. J. MacGowan, M. M. Marinak, D. D. Meyerhofer, J. L. Milovich, K. A. Moreno, E. I. Moses, D. H. Munro, A. Nikroo, R. E. Olson, K. Peterson, S. M. Pollaine, J. E. Ralph, H. F. Robey, B. K. Spears, P. T. Springer, L. J. Suter, C. A. Thomas, R. P. Town, R. Vesey, S. V. Weber, H. L. Wilkens, and D. C Wilson, Phys. Plamas **18**, 051001(2011).

17A. N. Simakov, D. C. Wilson, S. A. Yi, J. L. Kline, D. S. Clark, J. L. Milovich, J. D. Salmonson, and S. H. Batha, Phys. Plasmas, 21, 022701 (2014).

18J. L. Kline, S. A. Yi, A. N. Simakov, R. E. Olson, D. C. Wilson, G. A. Kyrala, T. S. Perry, S. H. Batha, A. B. Zylstra, E. L. Dewald, R. Tommasini, J. E. Ralph, D. J. Strozzi, A. G. MacPhee, D. A. Callahan, D. E. Hinkel, O. A. Hurricane, J. L. Milovich, J. R. Rygg, S. F. Khan, S. W. Haan, P. M. Celliers, D. S. Clark, B. A. Hammel, B. Kozioziemski, M. B. Schneider, M. M. Marinak, H. G. Rinderknecht, H. F. Robey, J. D. Salmonson, P. K. Patel, T. Ma, M. J. Edwards, M. Stadermann, S. Baxamusa, C. Alford, M. Wang, A. Nikroo, N. Rice, D. Hoover, K. P.Youngblood, H. Xu, H. Huang, and H. Sio, Phys. Plasmas, 23, 056310 (2016).

19A. J. MacKinnon, N. B. Meezan, J. S. Ross, S. Le Pape, L. Berzak Hopkiins, L. Divol, D. Ho, J. Milovich, A. Pak, J. Ralph, T. Döppner, P. K. Patel, C. Thomas, R. Tommasini, S. Haan, A. G. MacPhee, J. McNaney, J. Caggiano, R. Hatarik, R. Bionta, T. Ma, B. Spears, J. R. Rygg, L. R. Benedetti, R. P. J. Town, D. K. Bradley, E. L. Dewald, D. Fittinghoff, O. S. Jones, H. R. Robey, J. D. Moody, S. Khan, D. A. Callahan, A. Hamza, J. Biener, P. M. Celliers, D. G. Braun, D. J. Erskine, S. T. Prisbrey, R. J. Wallace, B. Kozioziemski, R. Dylla-Spears, J. Sater, G. Collins, E. Storm, W. Hsing, O. Landen, J. L. Atherton, J. D. Lindl, M. J. Edwards, J. A. Frenje, M. Gatu-Johnson, C. K. Li, R. Petrasso, H. Rinderknecht, M. Rosenberg, F. H. Séguin, A. Zylstra, J. P. Knauer, G. Grim, N. Guler, F. Merrill, R. Olson, G. A. Kyrala, J. D. Kilkenny, A. Nikroo, K. Moreno, D. E. Hoover, C. Wild, and E. Werner, Phys. Plasmas, 21, 056318 (2014).

20N. B. Meezan, L. F. Berzak Hopkins, S. Le Pape, L. Divol, A. J. MacKinnon, T. Doppner, D. D. Ho, O. S. Jones, S. F. Khan, T. Ma, J. L. Milovich, A. E. Pak, J. S. Ross, C. A. Thomas, L. R. Benedetti, D. K. Bradley, P. M. Celliers, D. S. Clark, J. E. Field, S. W. Haan, N. Izumi, G. A. Kyrala,J. D. Moody, P. K. Patel, J. E. Ralph, J. R. Rygg,1S. M. Sepke, B. K. Spears, R. Tommasini, R. P. J. Town, J. Biener, R. M. Bionta, E. J. Bond, J. A. Caggiano, M. J. Eckart, M. Gatu Johnson, G. P. Grim, A. V. Hamza, E. P. Hartouni, R. Hatarik, D. E. Hoover, J. D.

Kilkenny, B. J. Kozioziemski, J. J. Kroll, J. M. McNaney, A. Nikroo, D. B. Sayre, M. Stadermann, C. Wild, B. E. Yoxall, O. L. Landen, W. W. Hsing, and M. J. Edwards, Phys. Plasmas, **22**, 062703 (2015).

21G. N. Hall, O. S. Jones, D. J. Strozzi, J. D. Moody, D. Turnbull, J. Ralph, P. A. Michel, M. Hohenberger, A. S. Moore, O. L. Landen, L. Divol, D. K. Bradley,D. E. Hinkel, A. J. Mackinnon, R. P. J. Town, N. B. Meezan, L. Berzak Hopkins, and N. Izumi, Phys. Plasmas, 24, 062706 (2017).

22O. S. Jones, L. J. Suter, H. A. Scott, M. A. Barrios, W. A. Farmer,S. B.Hansen, D. A.Liedahl, C. W. Mauche, A. S.Moore, M. D.Rosen, J. D.Salmonson, D. J.Strozzi, C. A.Thomas, and D. P.Turnbull, Phys. Plasmas, 24, 056312 (2017).

23E. L. Dewald, O. L. Landen, J. Salmonson, L. Masse, M. Tabak, V. A. Smalyuk, S. Schiaffino, R. Heredia,
M. Schneider, and A. Nikroo, Phys. Plasmas 27, 122703 (2020).

24Hui Chen, D. T. Woods, O. S. Jones, L. R. Benedetti, E. L. Dewald, N. Izumi, S. A. MacLaren, N. B. Meezan, J. D. Moody, N. E. Palmer, M. B. Schneider, and M. Vandenboomgaerde, Phys. Plasmas, 27, 022702 (2020).

25 N B Meezan, M J Edwards, O A Hurricane, P K Patel, D A Callahan,
W W Hsing, R P J Town, F Albert, P A Amendt, L F Berzak Hopkins,
D K Bradley, D T Casey, D S Clark, E L Dewald, T R Dittrich, L Divol,
T Döppner, J E Field, S W Haan, G N Hall, B A Hammel, D E Hinkel,
D D Ho, M Hohenberger, N Izumi, O S Jones, S F Khan, J L Kline,
A L Kritcher, O L Landen, S LePape, T Ma, A J MacKinnon,
A G MacPhee, L Masse, J L Milovich, A Nikroo, A Pak, H-S Park,
J L Peterson, H F Robey, J S Ross, J D Salmonson, V A Smalyuk,
B K Spears, M Stadermann, L J Suter, C A Thomas, R Tommasini,
D P Turnbull and C R Weber, Plasma Control. Fusion 59 014021 (2017).

26 H. G. Rinderknecht, P. A. AMendt, S. C. Wilks, and G. Colins, Plasma Phys. Control. Fusion, 60 064001 (2018).

27 V.A. Smalyuk, C.R. Weber, O.L. Landen, S. Ali, B. Bachmann, P.M. Celliers, E. Dewald, A. Fernandez, B.A. Hammel, G. Hall, A.G. MacPhee, L. Pickworth, H.F. Robey, N. Alfonso, K.L. Baker, L.F. Berzak Hopkins, L. Carlson, D.T. Casey, D.S. Clark, J. Crippen, L. Divol, T. Doppner, J. Edwards, M. Farrell, S. Felker, J.E. Field, S.W. Haan, A.V. Hamza, M. Havre, M.C. Herrmann, W.W. Hsing, S. Khan, J. Kline, J.J. Kroll, S. LePape, E. Loomis, B.J. MacGowan, D. Martinez, L. Masse, M. Mauldin, J.L. Milovich, A.S. Moore, A. Nikroo, A. Pak, P.K. Patel, J.L. Peterson, K. Raman, B.A. Remington, N. Rice, M. Schoff, M. Stadermann, S.A. Yi, High Energy Density Physics 36,100820 (2020).

28C. A. Thomas, E. M. Campbell, K. L. Baker, D. T. Casey, M. Hohenberger, A. L. Kritcher, B. K. Spears, S. F. Khan, R. Nora, D. T. Woods, J. L. Milovich, R. L. Berger, D. Strozzi, D. D. Ho, D. Clark, B. Bachmann, L. R. Benedetti, R. Bionta, P. M. Celliers, D. N. Fittinghoff, G. Grim, R. Hatarik, N. Izumi, G. Kyrala, T. Ma, M. Millot, S. R. Nagel, P. K. Patel, C. Yeamans, A. Nikroo, M. Tabak, M. Gatu Johnson, P. L. Volegov, and S. M. Finnegan, Phys. Plasmas 27, 112705 (2020).

29H. F. Robey, L. Berzak Hopkins, J. L. Milovich, and N. B. Meezan, Phys. Plasmas, 25, 012711 (2018).

30K. L. Baker, C. A. Thomas, D. T. Casey, S. Khan, B. K. Spears, R. Nora, T. Woods, J. L. Milovich, R. L. Bergen, D. Strozzi, D. Clark, M. Hohenberger, O. A. Hurricane, D. A. Callahan, O. L. Landen, B. Bachmann, R. Benedetti, R. Bionta, P. M. Celliers, D. Fittinghoff, C. Goyon, G. Grim, R. Hatarik, N. Izumi, M. Gatu Johnson, G. Kyrala, T. Ma, M. Millot, S. R. Nagel, A. Pak, P. K. Patel, D. Turnbull, P. L. Volegov, and C. Yeamans, Phys. Rev. Lett., **121**, 135001 (2018).

31K. R. Manes, M. L. Spaeth, J. J. Adams, M. W. Bowers, J. D. Bude, C. W.Carr, A. D. Conder, D. A. Cross, S. G. Demos, J. M. G. Di Nicola, S. N. Dixit, E. Feigenbaum,R. G. Finucane, G. M. Guss, M. A. Henesian, J. Honig, D. H. Kalantar, L. M. Kegelmeyer, Z. M. Liao, B. J. MacGowan, M. J. Matthews, K. P. McCandless, N. C. Mehta, P. E. Miller, R. A. Negres, M. A. Norton, M. C. Nostrand, C. D. Orth, R. A. Sacks, M. J. Shaw, L. R. Siegel, C. J. Stolz, T. I.Suratwala, J. B. Trenholme, P. J. Wegner, P. K. Whitman, C. C. Widmayer and S. T. Yang, Fusion Science and Technology, **69**, 146-249 (2016).

32W. Carr, private communication (2007).

33D. S. Montgomery, W. S. Daughton, B. J. Albright, A. N. Simakov, D. C. Wilson, E. S. Dodd, R. C. Kirkpatrick, R. G. Watt, M. A. Gunderson, E. N. Loomis, E. C. Merritt, T. Cardenas, P. Amendt, J. L. Milovich, H. F. Robery, R. E. Tipton, and M. D. Rosen, Phys. Plasmas, **25**, 092706 (2018).

34M. M. MARINAK, S. W. HAAN, T. R. DITTRICH, R. E. TIPTON, AND G. B. ZIMMERMAN, PHYS. PLASMAS, 5, 1125 (1998).

35M. D. Rosen, H. A. Scott, D. E. Hinkel, E. A. Williams, D. A. Callahan, R. P. J. Town, L. Divol, P. A. Michel, W. L. Kruer, L. J. Suter, R. A. London, J. A. Harte, and G. B. Zimmerman, High Energy Density Phys. 7, 180 (2011).

36 R. Nora, R. Betti, K. S. Anderson, A. Shvydky, A. Bose, K. M. Woo, A. R. Christopherson, J. A. Marozas, T. J. B. Collins, P. B. Radha, S. X. Hu, R. Epstein, F. J. Marshall, R. L. McCrory, T. C. Sangster, and D. D. Meyerhofer, Phys. Plasmas, 21, 056316 (2014)

37O. A. Hurricane, D. A. Callahan, P. T. Springer, M. J. Edwards, P. Patel, K. Baker, D. T. Casey, L. Divol, T. Doppner, D. E. Hiinkel, L. F. Berzak Hopkins, A. Kritcher, S. Le Pape, S.

Maclaren, L. Masse, A. Pak, L. Pickworth, J. Ralph, C. Thomas, A. Yi, and A. Zylstra, Plasma Phys. Control. Fusion **61**, 014033 (2019).

38 M. D. Rosen, "Fundamentals of ICF Hohlraums", chapter in *Laser-Plasma Interactions*, 1st ed, (CRC Press, Boca Raton, Florida ,2009).

39O. S. Jones, C. J. Cerjan, M. M. Marinak, J. L. Milovich, H. F. Robey, P. T. Springer, L. R. Benedetti, D. L. Bleuel, E. J. Bond, D. K. Bradley, D. A. Callahan, J. A. Caggiano, P. M. Celliers, D. S. Clark, S. M. Dixit, T. Doppner, R. J. Dylla-Spears, E. G. Dzentitis, D. R. Farley, S. M. Glenn, S. H. Glenzer, S. W. Haan, B. J. Haid, C. A. Haynam, D. G. Hicks, B. J. Kozioziemski, K. N. LaFortune, O. L. Landen, E. R. Mapoles, A. J. MacKinnon, J. M. McNaney, N. B. Meezan, P. A. Michel, J. D. Moody, M. J. Moran, D. H. Munro, M. V. Patel, T. G. Parham, J. D. Sater, S. M. Sepke, B. K. Spears, R. P. J. Town, S. V. Weber, K. Widmann, C. C. Widmayer, E. A. Williams, L. J. Atherton, M. J. Edwards, J. D. Lindl, B. J. MacGowan, L. J. Suter, R. E. Olson, H. W. Herrmann, J. L. Kline, G. A. Kyrala, D. C. Wilson, J. Frenje, T. R. Boehly, V. Glebov, J. P. Knauer, A. Nikroo, H. Wilkens, and J. D. Kilkenny, Phys. Plasmas, **19**, 056315 (2012).

40P. Michel, L. Divol, E. A. Williams, S. Weber, C.A. Thomas, D. A. Callahan, S.W. Haan, J. D. Salmonson, S. Dixit, D. E. Hinkel, M. J. Edwards, B. J. MacGowan, J. D. Lindl, S. H. Glenzer, and L. J. Suter, Phys. Rev. Let. **102**, 025004 (2009).

41A. L. Kritcher, H. Robey, C. Young, and R. Olson, Phys. Plasmas 27, 082708 (2020).

42D. S. Clark, C. R. Weber, J. L. Milovich, A. E. Pak, D. T. Casey, B. A. Hammel, D. D. Ho, O. S. Jones, J. M. Koning, A. L. Kritcher, M. M. Marinak, L. P. Masse, D. H. Munro, M. V. Patel, P. K. Patel, H. F. Robey, C. R. Schroeder, S. M. Sepke, and M. J. Edwards, Phys. Plasmas **26**, 050601 (2019).

43V A Smalyuk, C R Weber, O L Landen, S Ali, B Bachmann, P M Celliers, E L Dewald, A Fernandez, B A Hammel, G Hall, A G MacPhee, L Pickworth, H F Robey, N Alfonso, K L Baker, L F Berzak Hopkins, L Carlson, D T Casey, D S Clark, J Crippen, L Divol, T Döppner, M J Edwards, M Farrell, S Felker, J E Field , S W Haan, A V Hamza, M Havre, M C Herrmann, W W Hsing, S Khan, J Kline, J J Kroll, S LePape, E Loomis, B J MacGowan, D Martinez, L Masse, M Mauldin, J L Milovich, A S Moore, A Nikroo, A Pak, P K Patel, J L Peterson, K Raman, B A Remington, N Rice, M Schoff and M Stadermann, Plasma Phys. Control. Fusion, **62**, 014007 (2020).

44 C. R. Weber, D. S. Clark, A. Pak, N. Alfonso, B. Bachmann, L. F. Berzak Hopkins, T. Bunn, J. Crippen, L. Divol, T. Dittrich, A. L. Kritcher, O. L. Landen, S. Le Pape, A. G. MacPhee, E. Marley, L. P. Masse, J. L. Milovich, A. Nikroo, P. K. Patel, L. A. Pickworth, N. Rice, V. A. Smalyuk, and M. Stadermann, Phys. Plasmas 27, 032703 (2020)

45 T. Ma, O. A. Hurricane, D. A. Callahan, M. A. Barrios, D. T. Casey, E. L. Dewald, T. R. Dittrich, T. Döppner, S.W. Haan, D. E. Hinkel, L. F. Berzak Hopkins, S. Le Pape, A. G. MacPhee, A. Pak, H.-S. Park, P. K. Patel, B. A. Remington, H. F. Robey, J. D. Salmonson, P. T. Springer, R. Tommasini, L. R. Benedetti, R. Bionta, E. Bond, D. K. Bradley, J. Caggiano, P. Celliers, C. J. Cerjan, J. A. Church, S. Dixit, R. Dylla-Spears, D. Edgell, M. J. Edwards, J. Field, D. N. Fittinghoff, J. A. Frenje, M. Gatu Johnson, G. Grim, N. Guler, R. Hatarik, H.W. Herrmann, W.W. Hsing, N. Izumi, O. S. Jones, S. F. Khan, J. D. Kilkenny, J. Knauer, T. Kohut, B. Kozioziemski, A. Kritcher, G. Kyrala, O. L. Landen, B. J. MacGowan, A. J. Mackinnon, N. B. Meezan, F. E. Merrill, J. D. Moody, S. R. Nagel, A. Nikroo, T. Parham, J. E. Ralph, M. D. Rosen, J. R. Rygg, J. Sater, D. Sayre, M. B. Schneider, D. Shaughnessy, B. K. Spears, R. P. J. Town, P. L. Volegov, A. Wan, K. Widmann, C. H. Wilde, and C. Yeamans, Phys. Rev. Lett., 114, 145004 (2015).

46 W. S. Varnum, N. D. Delameter, S. C. Evans, P. L. Gobby, J. E. Moore, J. M. Wallace, R. G. Watt, J. D. Colvin, R. Turner, V. Glebov, J. Soures, and C. Stoeckl, Phys. Rev. Lett. 84, 5153 (2000).

47 P. Amendt, J. D. Colvin, R. E. Tipton, D. E. Hinkel, M. J. Edwards, O. L. Landen, J. D. Ramshaw, L. J. Suter, W. S. Varnum, and R. G. Watt, Phys. Plasmas 9, 2221 (2002).

48J. L. Milovich, P. Amendt, M. Marinak, and H. Robey, Phys. Plasmas 11, 1552 (2004).

49K. Molvig, M. J. Schmitt, B. J. Albright, E. S. Dodd, N. M. Hoffman, G. H. McCall, and S. D. Ramsey, Phys. Rev. Lett. 116, 25503 (2016).

50E. Merritt, J. Sauppe, E. Loomis, T. Cardenas, D. Montgomery, W. Daughton, D. C. Wilson, J. Kline, S. Khan, M. Schoff, M. Hoppe, F. Fierro, B. Randolph, B. Patterson, L. Kuettner, R. Sacks, E. Dodd, W. C. Wan, S. Palaniyappan, S. Batha, P. Keiter, J. Rygg, V. Smalyuk, Y. Ping, and P. Amendt, *Phys. Plasmas*, **26**, 052702, (2019).

51S. H. Batha, K. S. Bradley, H. A. Baldis, R. P. Drake, K. Estabrook, T. W. Johnston, and D. S. Montgomery, *Phys. Rev. Letters*, **70**, 802 (1993).

52K. J. Bowers, B. J. Albright, B. Bergen, and T. J. T. Kwan, *Phys. Plasmas* **15**, 055703 (2008). Code available at https://github.com/lanl/vpic.

53K. J. Bowers, B. J. Albright, B. Bergen, L. Yin, K. J. Barker, and D. J. Kerbyson, in Proceedings of the ACM/IEEE Conference on Supercomputing, Austin (IEEE Press, Piscataway, NJ, USA, 2008), pp. 1–11.

54K. J. Bowers, B. J. Albright, L. Yin, W. Daughton, V. Roytershteyn, B. Bergen, and T. J. T. Kwan, J. Phys.: Conf. Ser. **180**, 012055 (2009).

55L. Yin, B. J. Albright, H. A. Rose, K. J. Bowers, B. Bergen, and R. K. Kirkwood, Phys. Rev. Lett. **108**, 245004 (2012).

56R. K. Kirkwood,P. Michel, R. London, J. D. Moody, E. Dewald, L. Yin,2 J. Kline, D. Hinkel, D. Callahan, N. Meezan, E. Williams, L. Divol, B. L. Albright, K. J. Bowers, E. Bond, H. Rose, Y. Ping, T. L. Wang, C. Joshi, W. Seka, N. J. Fisch D. Turnbull, S. Suckewer, J. S. Wurtele, S. Glenzer, L. Suter, C. Haynam, O. Landen, and B. J. Macgowan, Phys. Plasmas, 18, 056311 (2011).

57 R K Kirkwood, J D Moody, J Kline, E Dewald, S Glenzer, L Divol, P Michel, D Hinkel, R Berger, E Williams, J Milovich, L Yin, H Rose, B MacGowan, O Landen, M Rosen and J Lindl, Plasmas Phys. Control. Fusion 55, 103001 (2013)

58L. Yin, B. J. Albright, H. A. Rose, K. J. Bowers, B. Bergen, R. K. Kirkwood, D. E. Hinkel, A. B. Langdon, Michel, D. S. Montgomery, and J. L. Kline, Phys. Plasmas **19**, 056304 (2012).

59William L. Kruer, *The Physics of Laser Plasma Interactions*, p. 79 (Addison Wesley; New York; 1988).

60 L. Yin,1, B. J. Albright, H. A. Rose, D. S. Montgomery, J. L. Kline, R. K. Kirkwood, J. Milovich, S. M. Finnegan, B. Bergen, and K. J. Bowers, Phys. Plasmas, 21, 092707 (2014)

61L. Yin, B. J. Albright, D. J. Stark, W. D. Nystrom, R. F. Bird, and K. J. Bowers, Phys. Plasmas **26**, 082708 (2019).

62D. Eimerl, W. L. Kruer, and E. M. Campbell, Comments o Plasma Physics and Controlled Fusion, **15**(2), 85-104, (1992).

63J-M. G. Di Nicola, (private communication, 2020).

63 D. Eimerl, D. Milam, and J. Yu, Phys. Rev. Let., **70**, 2738 (1993).

65 J. W. Bates, J. F. Myatt, J. G. Shaw, R. K. Follett, J. L. Weaver, R. H. Lehmberg, and S. P. Obenschain, Phy. Rev. E, 97, 061202 (2018).

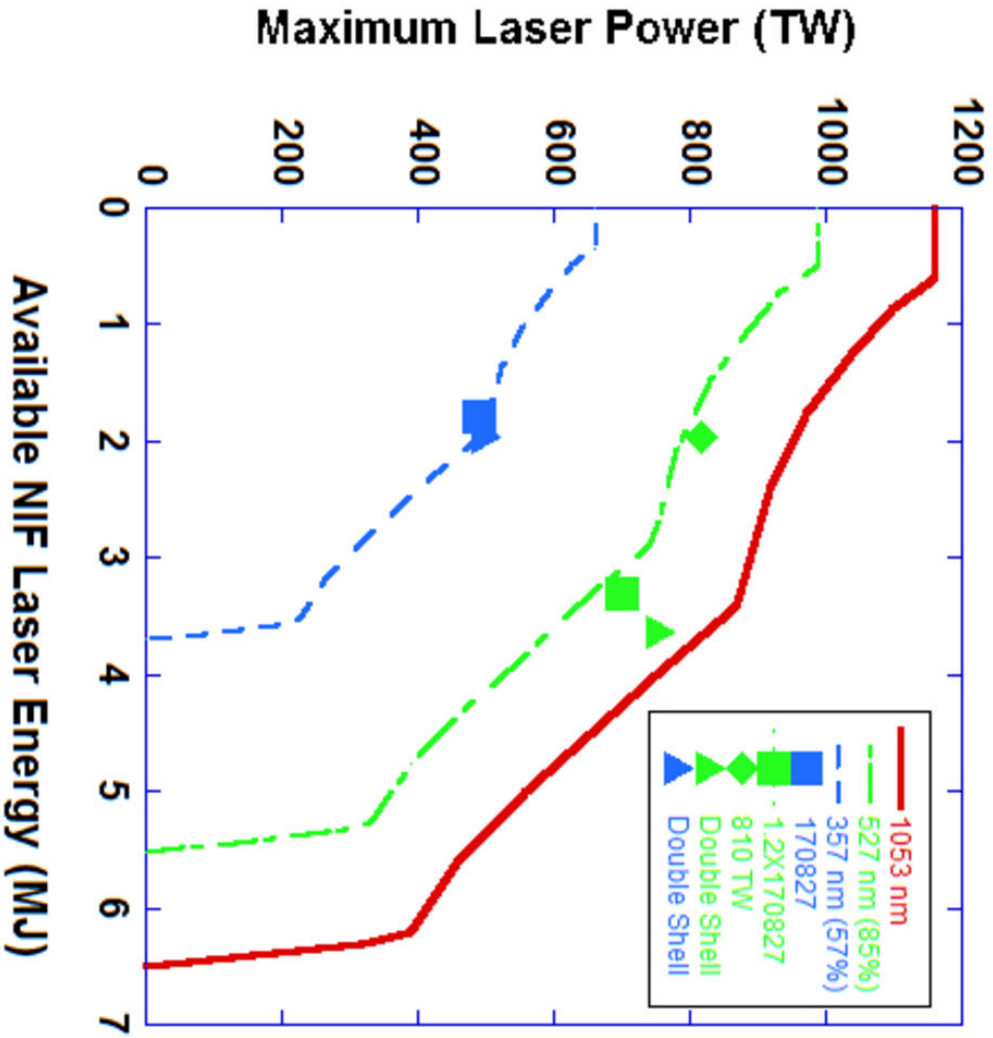

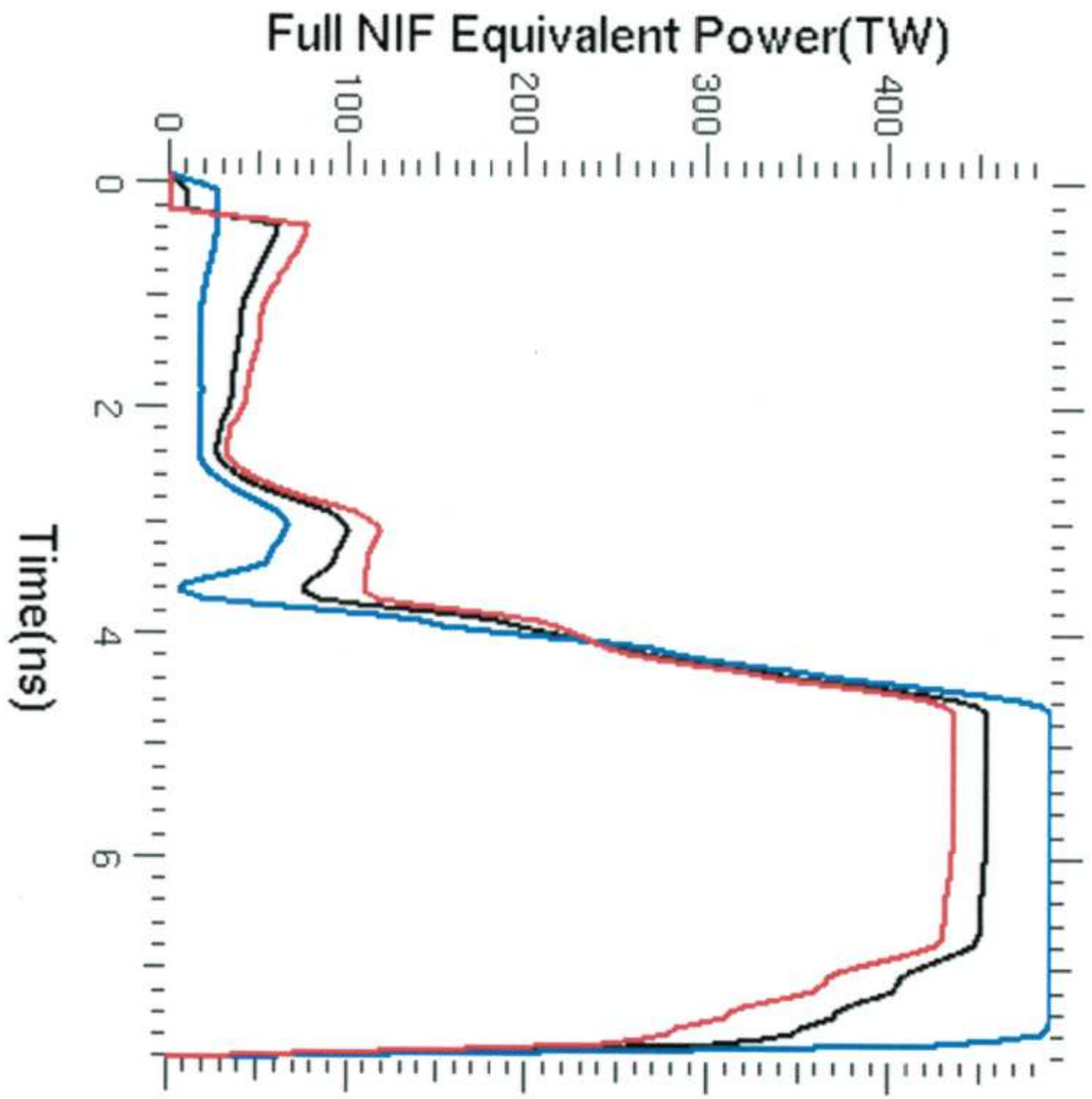

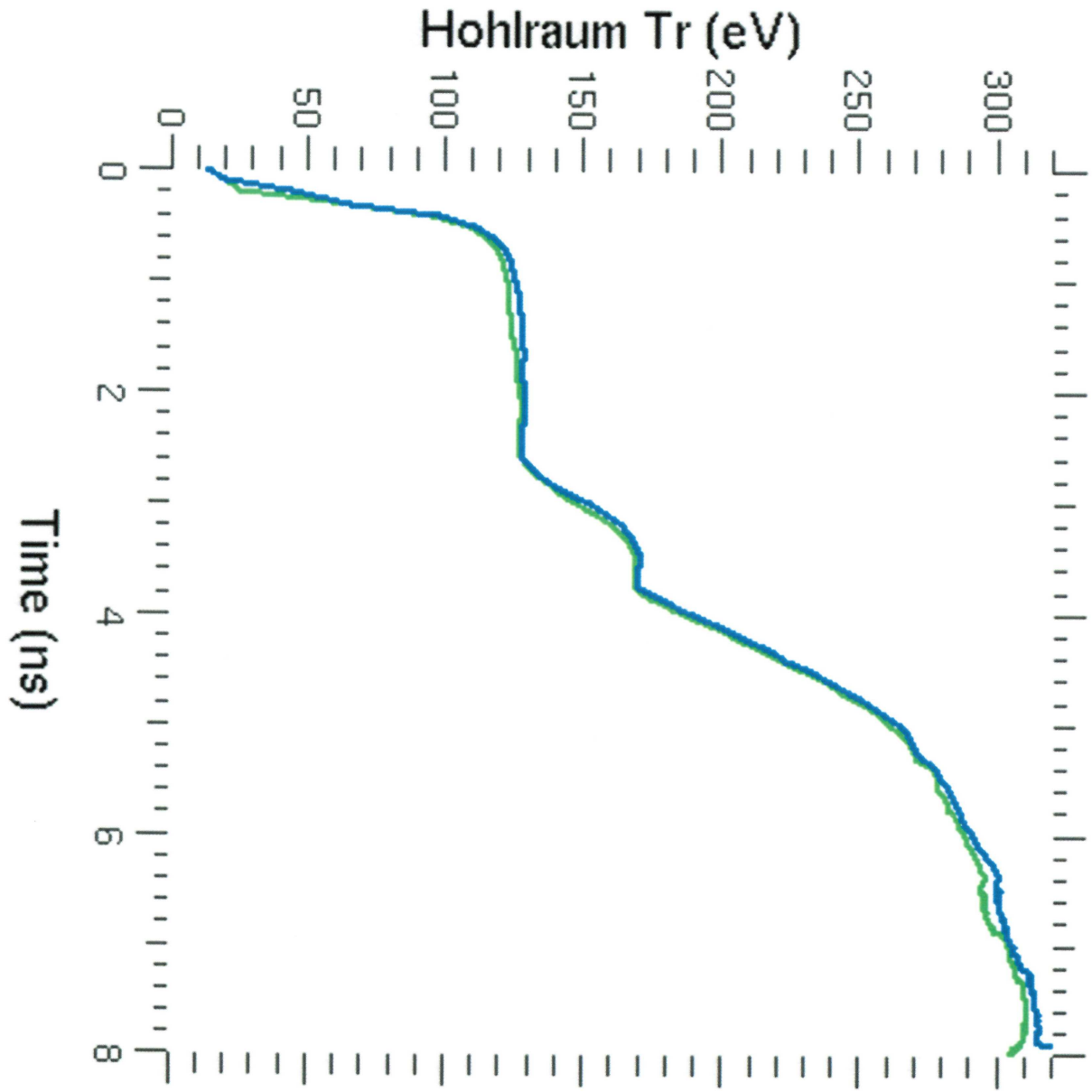

PLEASE CITE THIS ARTICLE AS DOI: 10.1063/5.0037338

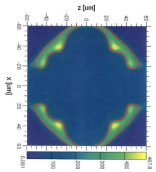

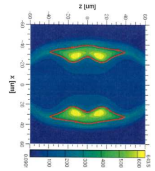

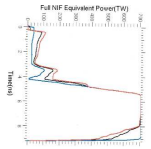

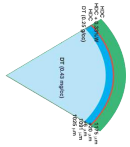

PLEASE CITE THIS ARTICLE AS DOI: 10.1063/5.0037338